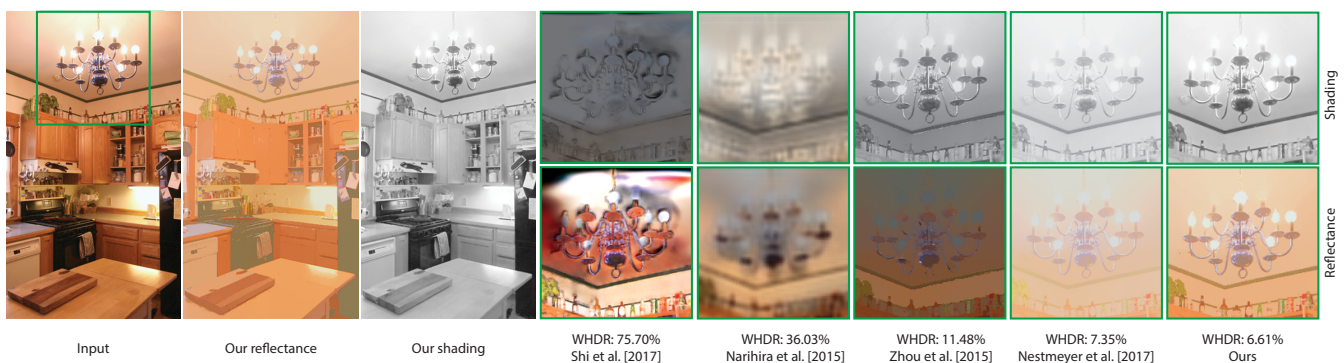


# Deep Hybrid Real and Synthetic Training for Intrinsic Decomposition

Sai Bi, Nima Khademi Kalantari, Ravi Ramamoorthi

University of California, San Diego



**Figure 1:** Our method decomposes an input image into intrinsic reflectance and shading layers. We propose a novel hybrid learning approach to train a convolutional neural network (CNN) on both synthetic and real images. To utilize the real images, we rely on the fact that two images of a scene captured with different lightings have the same reflectance, and thus, enforce that the network produces consistent results for the real image pairs during training. Here, we compare our approach against several state-of-the-art methods on a test image from the IIW dataset [BBS14]. Note that our system is not trained on this dataset. The deep learning (DL) approaches by Narihira et al. [NMY15] and Shi et al. [SDSS17] train a CNN only on synthetic data, and thus, are not able to produce reasonable results on real images because of the large gap in data distributions. Although the learning-based (non-DL) methods by Zhou et al. [ZKE15] and Nestmeyer and Gehler [NG17] specifically train their system on the IIW dataset, they are not able to handle the large shading variations in this scene. Note the brightness inconsistency of the ceiling in their reflectance insets. In comparison, our hybrid training approach is able to generate better results both visually and numerically, in terms of WHDR scores [BBS14] (lower is better). Note that the WHDR scores are calculated on the full images. See supplementary materials for the full images. We also compare against non-learning approaches in Table 1 and Fig. 9.

## Abstract

Intrinsic image decomposition is the process of separating the reflectance and shading layers of an image, which is a challenging and underdetermined problem. In this paper, we propose to systematically address this problem using a deep convolutional neural network (CNN). Although deep learning (DL) has been recently used to handle this application, the current DL methods train the network only on synthetic images as obtaining ground truth reflectance and shading for real images is difficult. Therefore, these methods fail to produce reasonable results on real images and often perform worse than the non-DL techniques. We overcome this limitation by proposing a novel hybrid approach to train our network on both synthetic and real images. Specifically, in addition to directly supervising the network using synthetic images, we train the network by enforcing it to produce the same reflectance for a pair of images of the same real-world scene with different illuminations. Furthermore, we improve the results by incorporating a bilateral solver layer into our system during both training and test stages. Experimental results show that our approach produces better results than the state-of-the-art DL and non-DL methods on various synthetic and real datasets both visually and numerically.

## CCS Concepts

• **Computing methodologies** → Computer graphics; Computer vision problems; Image processing; Neural networks;

## 1. Introduction

The visual appearance of objects in images is determined by the interactions between illumination and physical properties of the objects such as their materials. Separating an image into reflectance and shading layers is called intrinsic decomposition and has a wide range of computer graphics/vision applications [BKPB17], such as surface retexturing, scene relighting, and material recognition. The intrinsic image model states that the input image is the product of the reflectance and shading images, and thus, the problem of inferring these two images from the input image is heavily underdetermined.

A category of successful methods addresses this problem in a data-driven way. A few approaches [NMY15, SDSS17] propose to train a model only on synthetic images, like the one shown in Fig. 2-a, as obtaining ground truth reflectance and shading for real images is difficult. However, since the data distribution of synthetic and real images is different, these methods produce sub-optimal results on real images, as shown in Fig. 1. Although several approaches [ZKE15, NG17] train their system on real images from the IIW dataset [BBS14], this dataset only contains relative comparison over reflectance values at pixel pairs (see Fig. 2-b), which is not sufficient for training a reliable model. Therefore, these methods often are not able to fully separate shading from the reflectance, as shown in Fig. 1.

To address these problems, we propose a hybrid approach to train a convolutional neural network (CNN) on both synthetic and real images. Our main observation is that a pair of images of the same scene with different illumination (see Fig. 2-c) have the same reflectance. We use this property to train our network on real images by enforcing the CNN to produce the same reflectance for the pair of images. In our system, the synthetic data constrains the network to produce meaningful outputs, while the real data tunes the network to produce high-quality results on real-world images. To improve the spatial coherency of the results, we propose to incorporate a bilateral solver layer with our network during both the training and test stages. We extensively evaluate our approach on a variety of synthetic and real datasets and show significant improvement over state-of-the-art methods, both visually (Figs. 1 and 9) and numerically (Tables 1 and 3). In summary, we make the following contributions:

1. We propose a hybrid approach to train a CNN on both synthetic and real images (Sec. 3.1) to address the shortcomings of previous approaches that train their models only on synthetic data or on real images with limited pairwise comparisons.
2. We incorporate a bilateral solver layer into our network and train it in an end-to-end fashion to suppress the potential noise and improve the spatial coherency of the results (Sec. 3.2).

## 2. Related Work

Barrow and Tenenbaum [BT78] introduced the concept of intrinsic decomposition and showed that it is desirable and possible to describe a scene in terms of its intrinsic characteristics. Since then significant research has been done and many powerful approaches have been developed. Several methods have proposed

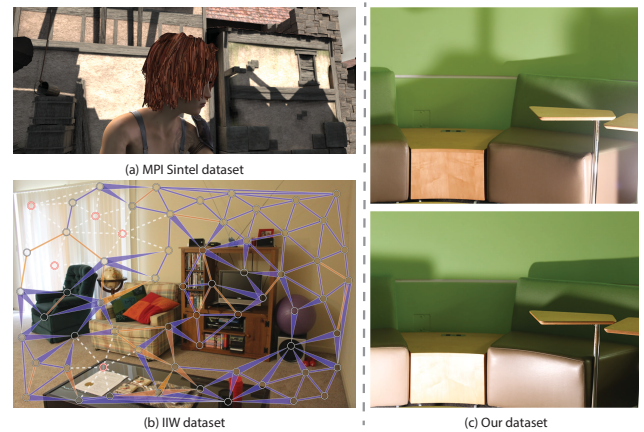


**Figure 2:** Several existing learning-based approaches train their system only on synthetic images (a), and thus, produce sub-optimal results on real images. Others use the pairwise relationships between reflectance values over pixel pairs from the IIW dataset (b), which is not sufficient to train a reliable model. On the other hand, we train our system on both synthetic images from the Sintel dataset and pairs of real world images of the same scene with different illuminations (c).

more complex imaging models and decompose the image into specular [SDSS17] or ambient occlusion [HWBS16, IRWM17] layers in addition to the typical reflectance and shading layers. Here, we consider a standard intrinsic image model, which covers the majority of real-world cases, and decompose the image into reflectance and shading layers. Moreover, several methods utilize additional information like depth [CK13], user interactions [BPD09], or use a collection of images [LBP\*12] to facilitate intrinsic decomposition. For brevity, we only focus on approaches that perform intrinsic decomposition on a single input image by categorizing them into two general classes of physical prior based and data-driven approaches.

*Physical Prior Based Approaches* – The approaches in this category use a physical prior in their optimization system to address this underdetermined problem. Retinex theory [LM71, Hor74], the most commonly-used prior, states that color changes caused by reflectance are generally abrupt, while those from shading variations are continuous and smooth. Based on this observation, Tappen et al. [TFA05] train a classifier to determine if the image derivative at each pixel is because of the shading or reflectance changes. Shen et al. [STL08] and Zhao et al. [ZTD\*12] observe that pixels with the same local texture configurations generally have the same reflectance values, and utilize this observation as a non-local constraint to reduce the number of unknowns when solving for reflectance. A couple of approaches [BST\*14, MZRT16] separate image derivatives into smooth shading variations and sparse reflectance changes by encoding the priors in a hybrid  $\ell_2$ - $\ell_p$  objective function. Zoran et al. [ZIKF15] train a network on the IIW dataset to predict the ordinal relationship of reflectance values between a pair of pixels and combine such constraints with Retinex theory to formulate a quadratic energy function.

Reflectance sparseness is another commonly-used prior, which states that there are a small number of different reflectance values in natural images [OW04]. Barron et al. [BM15] encode this prior in their optimization framework by minimizing the global entropy of log-reflectance. Garces et al. [GMLMG12], Bell et al. [BBS14] and Bi et al. [BHY15] sample a sparse set of reflectance values from the image and assign each pixel to a specific value with methods such as k-means clustering and conditional random field (CRF). Zhou et al. [ZKE15] further improve the CRF framework by replacing the handcrafted pairwise terms used to evaluate the similarity of pixel reflectance with the predictions of a neural network trained on the IIW dataset.

A common problem with the approaches mentioned above is that the priors are not general enough to cover a wide range of real world complex scenes. For example, shading smoothness does not always hold in practice due to the existence of depth discontinuities, occlusions, as well as abrupt surface normal changes. In this case, approaches based on these priors will inevitably generate incorrect decompositions. In contrast, our approach is fully data-driven and does not have these problems.

*Data-Driven Approaches* – Recently some approaches have tried to directly estimate the reflectance and shading by training a CNN. The major challenge is that obtaining ground truth reflectance and shading for real-world scenes is difficult. To overcome this limitation, approaches [NMY15, SDSS17] have been proposed to train a CNN on synthetic datasets, such as MPI Sintel [BWSB12] and ShapeNet [CFG\*15]. These approaches perform poorly on real images because of the large gap between the distribution of synthetic and real-world data. Nestmeyer and Gehler [NG17] train a network utilizing only pairwise ordinal relationships on reflectance values in the IIW dataset, which only contains sparse annotations over a small number of pixels. However, these pairwise comparisons do not provide sufficient supervision for the network to produce high-quality results in challenging cases (Figs. 1 and 9). We avoid these problems by proposing a novel approach to utilize real-world images for supervising the network and perform a hybrid training on both real and synthetic datasets.

### 3. Algorithm

The goal of our approach is to decompose an input image,  $I$ , into its corresponding reflectance,  $R$ , and shading,  $S$ , images. In our system, we consider the input image to be the product of the reflectance and shading layers, i.e.,  $I = R \cdot S$ . For simplicity we assume the scenes to have achromatic lighting (i.e.  $S$  is a single channel image) similar to the majority of existing techniques. However, extension to colored lighting is straightforward. Inspired by the success of deep learning in a variety of applications, we propose to model this complex process using a CNN. The key to success of every learning system lies in effective training and appropriate network architecture, which we discuss in Secs. 3.1 and 3.2, respectively.

#### 3.1. Training

As discussed, obtaining ground truth reflectance and shading images for real-world scenes is difficult. To overcome this limitation,

we make a key observation that two images of the same scene under different illuminations have the same reflectance. Based on this observation, we propose a novel approach to provide a weak supervision for the network by enforcing it to produce the same reflectance for pairs of real images. Although necessary, this weak supervision is not sufficient for training a reliable model, as shown in Fig. 3. Our main contribution is to propose a hybrid training on both synthetic and real images by minimizing the following loss:

$$E = E_{\text{syn}} + \omega E_{\text{real}}, \quad (1)$$

where  $E_{\text{syn}}$  and  $E_{\text{real}}$  are defined in Eqs. 2 and 4, respectively, and  $\omega$  defines the weight of the real loss. We set  $\omega$  to 0.5 to keep the real and synthetic losses within a reasonable range and avoid instability in training. Intuitively, training on synthetic images constrains the network to produce meaningful outputs, while the weak supervision on real images adapts the network to real-world scenes. Note that, as shown in Fig. 3, a network trained only on synthetic images does not generalize well to real images and both terms in Eq. 1 are necessary to produce high-quality results. Next, we discuss our synthetic ( $E_{\text{syn}}$ ) and real ( $E_{\text{real}}$ ) losses, as well as the training details and dataset.

*Synthetic Images* – Since the ground truth reflectance,  $\hat{R}$ , and shading,  $\hat{S}$ , images for a synthetic dataset are available, we can provide a direct supervision for the network by minimizing the mean squared error (MSE) between the ground truth and the estimated reflectance and shading layers. However, there exists an inherent scale ambiguity in intrinsic decomposition, i.e., if  $R$  and  $S$  are the true reflectance and shading images,  $\alpha R$  and  $S/\alpha$  are also valid. Therefore, we use the scale invariant MSE ( $E_{\text{si}}$ ) [EPF14] to measure the quality of our decomposition. Our synthetic loss is defined as follows:

$$E_{\text{syn}} = E_{\text{si}}(R, \hat{R}) + E_{\text{si}}(S, \hat{S}) + E_{\text{si}}(R \cdot S, I), \quad (2)$$

where the scale invariant loss is defined as:

$$E_{\text{si}}(\hat{M}, M) = \frac{1}{N} \|\hat{M} - \alpha M\|_2, \quad \text{where } \alpha = \underset{\alpha}{\operatorname{argmin}} \|\hat{M} - \alpha M\|_2. \quad (3)$$

Here,  $N$  is the number of elements in  $M$ , and  $\alpha$  is a scalar with an analytical solution  $\alpha = (\sum \hat{M} \cdot M) / (\sum M \cdot M)$ .

The first and second terms of Eq. 2 are necessary to enforce that the network produces similar results to the ground truth. Moreover, since our network estimates the reflectance and shading independently, we use the third term to enforce that the product of them is the same as the original input image. Note that since our estimated reflectance and shading could potentially have arbitrary scales, we also use a scale invariant MSE to compare their product with the input image.

*Real Image Pairs* – Since the ground truth reflectance and shading images are not available in this case, we propose to provide a weak supervision for training the network by enforcing it to produce the same reflectance for real image pairs. Specifically, given a

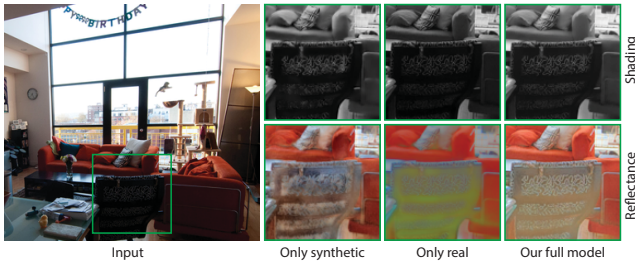


**Figure 3:** We analyze different terms in Eq. 1 by training the system on each term and comparing it to our full approach. As shown in the insets, the synthetic and real losses alone are not sufficient to produce high-quality results. Our approach minimizes both terms, and thus, produces reflectance and shading images with higher quality.

pair of real images taken of the same scene under different illuminations,  $I_1$  and  $I_2$ , we use our network to estimate their corresponding reflectance ( $R_1$  and  $R_2$ ) and shading ( $S_1$  and  $S_2$ ) images. We then optimize the following loss function to train our network:

$$E_{\text{real}} = E_{\text{si}}(R_1, R_2) + E_{\text{si}}(R_1 \cdot S_2, I_2) + E_{\text{si}}(R_2 \cdot S_1, I_1). \quad (4)$$

Here, the first term enforces that the network produces the same reflectance layers for the pair of real images. Note that we use the scale invariant MSE to reduce the complexity of training and avoid enforcing the network to unnecessarily resolve the scale ambiguity. This term only provides feedback for estimating reflectance on the real images, but we also need to supervise the network for estimating the shading.

We do so by introducing the second and third terms in Eq. 4. The basic idea behind these terms is that the product of the estimated reflectance and shading should be equal to the corresponding input image, e.g.,  $R_1 \cdot S_1 = I_1$ . Therefore, we can provide supervision by minimizing the error between the product of decomposed layers and the input image. Here, we swap the two reflectance images to further enforce the similarity of the estimated reflectance images. Note that, as in the synthetic loss, we use the scale invariant MSE as the estimated reflectance and shading could have arbitrary scales.

We note that existing methods [Wei01, LBP\*12] that use multiple images for intrinsic decomposition are fundamentally different from ours. These approaches always require multiple images to perform intrinsic decomposition. In contrast, we only use the image pairs during training and at the test time, our trained network works on a single image, and thus, is more practical.

*Training Details and Dataset* – Training a network from scratch on both synthetic and real images by minimizing Eq. 1 is challenging. Therefore, we propose to perform the training in two stages. First, we train the network only on synthetic images by minimizing the synthetic loss in Eq. 2. After convergence, the network is able to produce meaningful reflectance and shading images. This stage basically provides a good initialization for the second stage in which we train the network on both synthetic and real image pairs by minimizing our full loss in Eq. 1. The second stage refines the network

to generate more accurate reflectance and shading layers on real images, while preserving its accuracy on synthetic images.

For the synthetic dataset, we use the training images from the MPI Sintel, containing 440 images of size  $1024 \times 436$ . For the real images, we used a tripod mounted camera to take multiple images of a static scene by changing the illumination of the scene. In order to change the illumination, we use between one to four light sources and randomly moved them around the scene. We use this approach to take between 3 to 8 images with varying illumination of 40 scenes. Note that during every iteration of training we randomly choose only two images of each scene to minimize Eq. 1. Figure 4 shows image pairs of a few scenes from our training dataset. In Sec. 4, we demonstrate the performance of our approach on several real and synthetic scenes, none of them included in the training set.

To increase the efficiency of training, we randomly crop patches of size  $256 \times 256$  from the input images. In stage one of the training, we use mini-batches of size 4, while we perform hybrid training on mini-batches of size 8 (4 synthetic and 4 real). We implemented our network using the PyTorch framework, and used ADAM solver [KB14] to optimize the network with the default parameters ( $\beta_1 = 0.9, \beta_2 = 0.999$ ), and a learning rate of 0.0002. The training in the first and second stages converged after roughly 300K and 1.2M iterations, respectively. We used an Intel Core i7 with a GTX 1080Ti GPU to train our network for roughly two days.

### 3.2. Network Architecture

We use a CNN with encoder-decoder architecture to model the process, as shown in Fig. 5. Our network contains one encoder, but two decoders for estimating the reflectance and shading layers. The input to our network is a single color image with three channels, while the output reflectance and shading have three and one channel, respectively. Note that our estimated shading has a single channel since we assume that the lighting is achromatic, which is a commonly-used assumption [GRK\*11]. Since the Sintel images have colored shading, we first convert them to grayscale and then use them as ground truth shading for training our network.

As shown in Fig. 6 (without bilateral), the CNN by itself is not able to fully separate the shading from reflectance. This is because the synthetic Sintel dataset often contains images with low frequency reflectance layers. In contrast, the reflectance of real images is usually sparse. Therefore, training the network on this synthetic dataset encourages it to produce reflectance images with low frequency content. Note that although we provide a weak supervision on real images, it only constrains the network to produce the same reflectance for a pair of real images and does not specifically solve this problem.

We propose to address this issue by applying a bilateral solver [BP16] on the estimated reflectance images to remove the low frequency content, while preserving the sharp edges. This optimization-based approach is differentiable as well as efficient, and produces results with better quality [BP16] than simple bilateral filtering techniques [SB97, TM98].

Our contribution is to integrate this differentiable bilateral solver into our CNN as a layer (see Fig. 5) and use it during both training and testing. While the bilateral solver has been integrated into

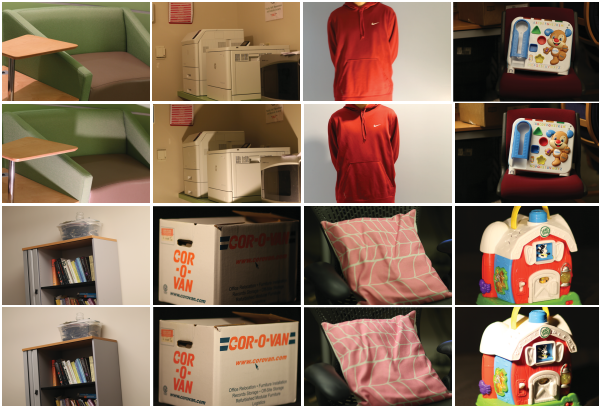


**Figure 4:** We show real image pairs for a few scenes from our training set. The images for each scene are obtained by changing the illumination.

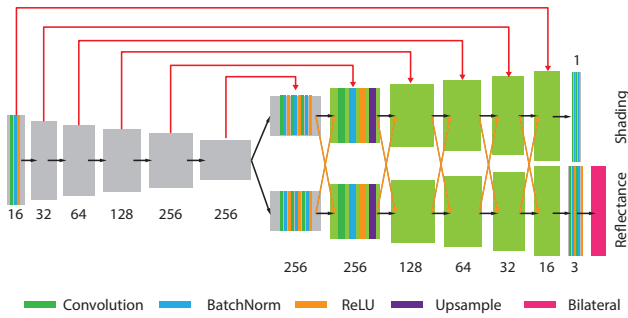


**Figure 5:** We use an encoder-decoder network with skip links to train our model. Each basic block in the encoder network consists of three types of layers, including convolutional layer, batch normalization layer, and Rectified Linear Unit (ReLU) layer. The basic block in the decoder network includes an extra bilinear upsampling layer to increase the spatial resolution of output.

CNNs for applications such as depth estimation [SGW\*18], our approach is the first to apply it for intrinsic decomposition. Previous techniques such as Nestmeyer et al. [NG17] use a bilateral filter in post-processing. In comparison, our whole network is trained in an end-to-end fashion. This integration is essential as it would encourage the network to focus on estimating the high frequency regions in the reflectance layer accurately and leaving the rest to the bilateral solver. Note that, as shown in Fig. 5, we only add this bilateral solver layer to the reflectance branch. Moreover, as discussed, the reflectance layer of the synthetic images usually has low frequency content, and thus, filtering the estimated reflectance on these images could potentially complicate the training. Therefore, we only apply the bilateral solver to the estimated reflectance for real images. Our final real loss is defined as:

$$E_{\text{real}} = E_{\text{si}}(R_1^*, R_2^*) + E_{\text{si}}(R_1^* \cdot S_2, I_2) + E_{\text{si}}(R_2^* \cdot S_1, I_1), \quad (5)$$

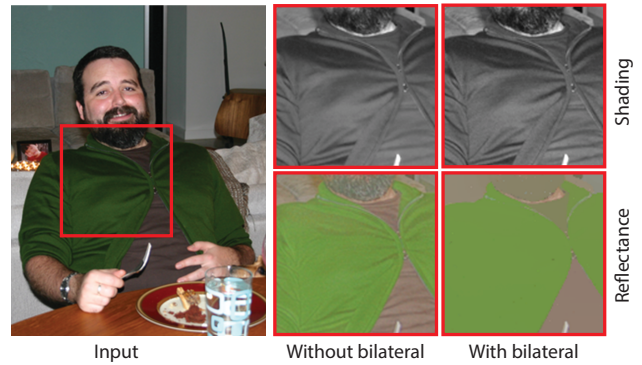


**Figure 6:** We compare the results generated using our models with and without the bilateral solver layer. The CNN by itself is not able to fully separate the shading from the reflectance and leaves the wrinkles on the shirt. Our full approach uses a bilateral solver to remove these low frequency shading variations from the reflectance image. See numerical evaluation of the effect of bilateral solver layer in Table. 1.

where  $R_1^*$  and  $R_2^*$  are the result of applying bilateral solver to the estimated reflectance layers,  $R_1$  and  $R_2$ .

In our system, the bilateral solver is formulated as follows:

$$R^* = \underset{\hat{R}}{\text{argmin}} \gamma \sum_{i,j} W(I_i, I_j) (\hat{R}_i - \hat{R}_j)^2 + \sum_i (\hat{R}_i - R_i)^2 \quad (6)$$

where  $W(I_i, I_j)$  is an exponential weight and is defined as:

$$W(I_i, I_j) = \exp(-\|\mathbf{f}_i - \mathbf{f}_j\|_2^2), \quad \text{where } \mathbf{f}_i = \left( \frac{x_i}{\sigma_x}, \frac{y_i}{\sigma_y}, \frac{l_i}{\sigma_l}, \frac{u_i}{\sigma_u}, \frac{v_i}{\sigma_v} \right) \quad (7)$$

Here,  $I$  is the input image,  $R$  is the estimated reflectance, and  $\gamma$  is a scalar that controls the smoothness of output, which we set to 12000.  $W$  calculates the affinity between a pair of pixels based on the features including spatial locations  $(x, y)$  and the pixel color in LUV color space  $(l, u, v)$ .  $\sigma_x$ ,  $\sigma_y$ ,  $\sigma_l$ ,  $\sigma_u$ , and  $\sigma_v$  determine the weight of each feature and we set them to 5, 5, 7, 3, and 3, respectively. Since the output is not differentiable with respect to these parameters, we use a numerical approach to find their values. Specifically, we filter our estimated reflectance image with a set of different parameters on 100 randomly chosen scenes from the IIW training set. We then choose the values that produce results with the lowest WHDR score.

Note that there are existing approaches that use conditional random fields (CRF) to smooth the reflectance labellings as a post-process [BBS14, BHY15] or integrate it into their learning model [ZJRP\*15]. However, these methods perform hard clustering on a pre-defined number of labels, and thus, produce significant artifacts in challenging cases, as shown in Figure 7.

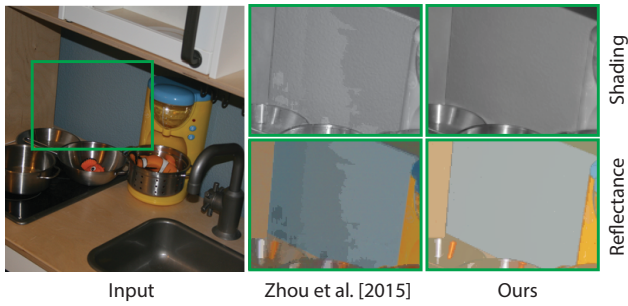


**Figure 7:** Zhou et al. [ZKE15] use a conditional random field (CRF) to cluster the reflectance pixels into a fixed number of labels. Therefore, their results often contain artifacts because of incorrect clustering, as shown in the insets. We avoid this problem by utilizing a bilateral solver to smooth the predicted reflectance image.

	Train on IIW	Median WHDR (%)	Mean WHDR (%)
Bell (2014)	✗	19.63	20.64
Bi (2015)	✗	16.42	17.67
Zhou (2015)	✓	19.13	19.95
Narihira (2015)	✗	40.52	40.90
Shi (2017)	✗	54.28	54.44
Nestmeyer (2017)	✓	16.71	17.69
<b>Ours: synthetic only</b>	✗	39.00	39.18
<b>Ours: real only</b>	✗	24.02	24.74
<b>Ours: synthetic + real</b>	✗	20.14	20.32
<b>Ours: full model</b>	✗	<b>15.86</b>	<b>17.18</b>
Zoran* (2015)	✓	16.55	17.85
<b>Ours*</b>	✗	<b>16.01</b>	<b>17.23</b>

**Table 1:** Quantitative comparison on IIW dataset in terms of WHDR score. Note that since Zoran et al. use a different training and testing split, their scores are not directly comparable to other methods. Therefore, we compare our method against their approach separately.

## 4. Results

In this section, we compare our approach against several state-of-the-art methods. Specifically, we compare against the non-learning approach of Bi et al. [BHY15], the learning-based (non-DL) methods by Zhou et al. [ZKE15], Zoran et al. [ZIKF15], and Nestmeyer and Gehler [NG17], and the DL algorithms by Narihira et al. [NMY15] and Shi et al. [SDSS17]. For all the approaches, we use the source code provided by the authors. We first show the results on real-world scenes (Sec. 4.1) and then demonstrate the performance of our approach on synthetic images (Sec. 4.2).

### 4.1. Comparisons on real images

*Comparison on IIW Dataset* – We begin by comparing our approach against the other methods on the IIW dataset [BBS14], which uses human judgments of reflectance comparisons on a set of sparse pixel pairs as the ground truth. We evaluate the quality

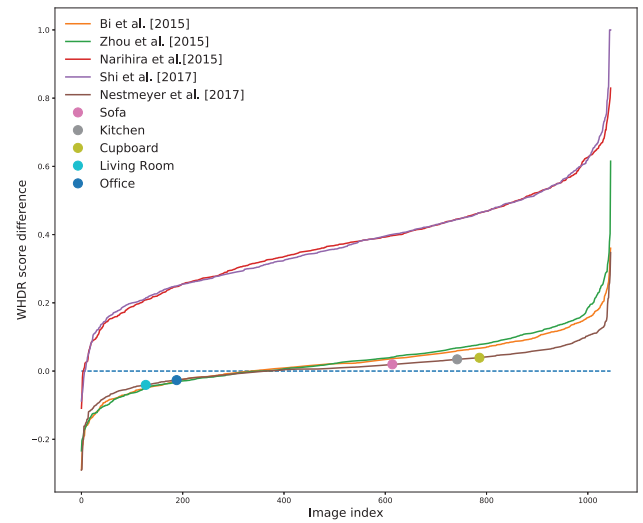


**Figure 8:** For each plot, we subtract our WHDR score from the score of the competing approach and sort the differences for the 1000 scenes in the IIW dataset in ascending order. Therefore, a particular image index corresponds to different images for each approach. Here, a positive difference shows that our approach is better. Our method produces better scores than all the other approaches in 65% of the cases. We mark the images, shown in Fig. 9, on the Nestmeyer et al.’s plot to demonstrate that the selected images represent the dataset.

of the estimated reflectance images for each algorithm using the weighted human disagreement rate (WHDR) [BBS14], as shown in Table 1. Although our method has not been specifically trained on this dataset, we produce the best (lower is better) WHDR scores compared to the other approaches. We also evaluate the effect of each term in Eq. 1 as well as the bilateral solver layer. As seen, training using both  $E_{syn}$  and  $E_{real}$  reduces the score to 20.32%, compared to the scores of 39.18% with synthetic images only and 24.74% with real images only. The bilateral solver layer in our full model further decreases the score from 20.32% to 17.18%. We also plot the WHDR score differences of our and other approaches for all the 1046 testing images in the IIW dataset in Fig. 8. As can be seen, our method produces better scores than all the other approaches on the majority of images.

Figure 9 compares our results against other approaches on five representative (see Fig. 8) scenes. Note that since Zoran et al.’s method uses a different training and testing split, we show comparison against their method separately in Fig. 10. The SOFA scene has complex shading variations on the surface of the sofa. The approaches by Bi et al. and Zhou et al. use a conditional random field (CRF) to assign a reflectance value to each pixel, and thus, their reflectance images contain sharp color changes because of incorrect labeling. Moreover, Zhou et al.’s method is not able to remove the wrinkles, produced by shading variations, from the sofa. Narihira et al. and Shi et al. train their model only on synthetic images, and thus, are not able to produce satisfactory results on real scenes. In

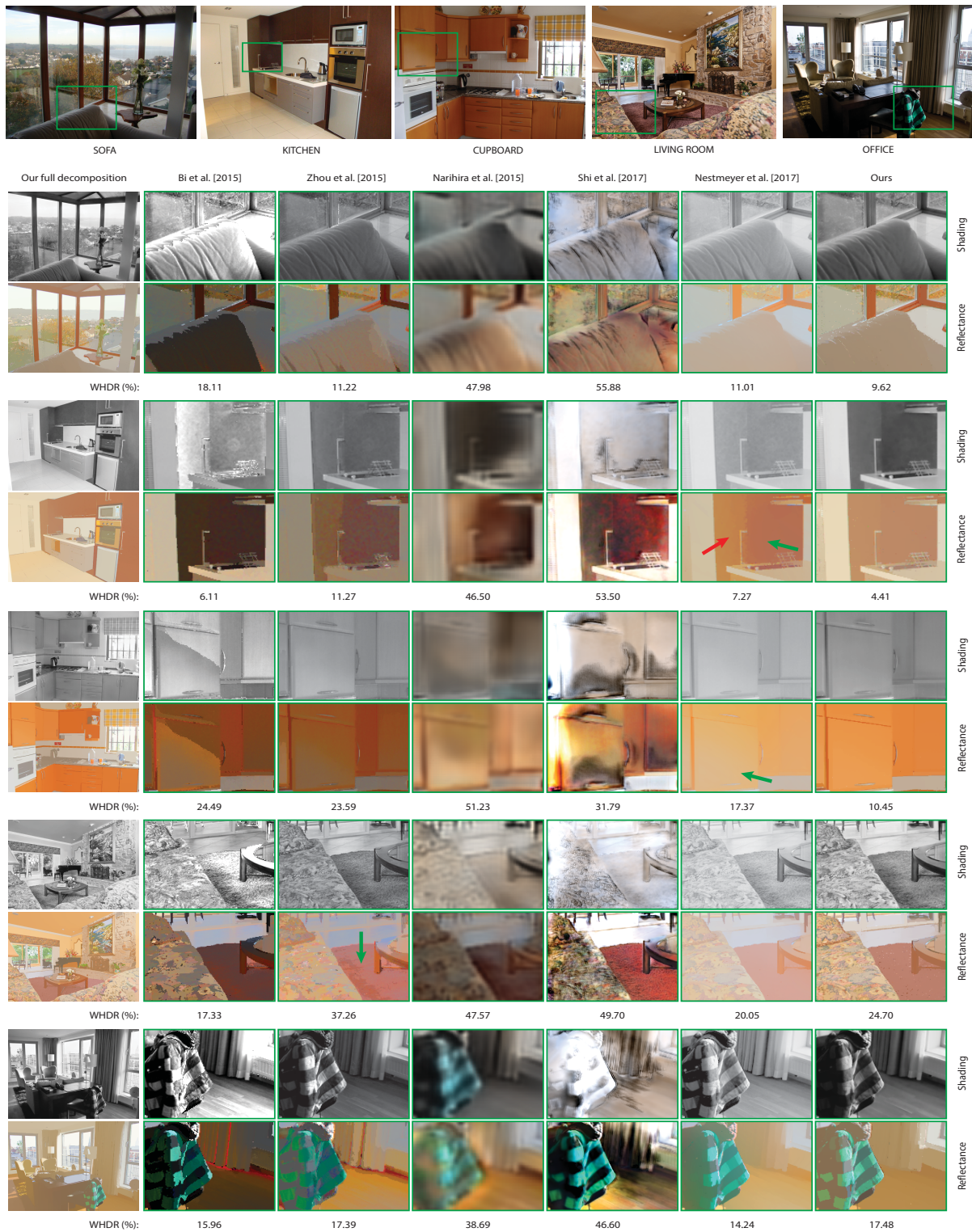


**Figure 9:** Comparison against several state-of-the-art approaches on the IIW dataset. The WHDR score for each method is listed below their results. Overall, our method produces visually and numerically better results than the other approaches. See supplementary materials for the full images.

this case, our approach produces better results than the other methods, but is comparable to Nestmeyer and Gehler’s method.

Although the two sides of the cupboard in the KITCHEN scene have the same reflectance, because of large normal variation, they have different pixel colors in the input image. While Bi et al.’s method is able to assign the correct label to the pixels in this region, their result suffers from inaccurate cluster boundaries, which can be clearly seen from the estimated shading. All the other approaches are not able to produce a reflectance image with the same color on the two sides of the cupboard. On the other hand, our method produces a high-quality decomposition.

The CUPBOARD scene has slight shading variations on the cabinet. None of the other approaches are able to fully separate the shading from reflectance. However, our method produces visually and numerically better results than other methods. For the LIVING ROOM and OFFICE scene, although our WHDR scores are slightly worse than some of the comparison methods, our method produces visually better results by preserving better texture details in reflectance and recovering correct shading information. The couch and carpet in the LIVING ROOM scene have complex textures and shading variations. Bi et al., Narihira et al. and Shi et al. cannot deal with such a challenging case and assign incorrect reflectance to the couch surface. Zhou et al. cannot deal with shading variations on the carpet and incorrectly preserves shading in reflectance. Nestmeyer et al. is able to handle the shading variations, but it also removes the high frequency details and generates an over-smoothed reflectance image. In comparison, our method is able to remove the shading variations and preserves the texture details at the same time. Finally, we examine the OFFICE scene, which contains large shadow areas. Despite having better WHDR scores, the estimated reflectance images by Bi et al. and Zhou et al. have severe artifacts in the shadow areas around the curtain. Narihira et al. and Shi et al. perform poorly on this challenging scene. Moreover, Nestmeyer and Gehler’s method is not able to properly handle the shadow areas on the left side of the jacket.

We compare our method against Zoran et al.’s algorithm in Fig. 10. Their method assumes that each superpixel in the image has constant reflectance. Therefore, in the BEDROOM scene, their estimated reflectance lacks details on the quilt and has color variations. Moreover, their method is not able to remove the shadows on the carpet from the reflectance image. In comparison, our method produces better results visually and numerically in both cases.

*Comparison on Illumination Invariance* – We evaluate the performance of all the methods on generating consistent reflectance layers from images with different illuminations. To do so, we use the dataset from Boyadzhiev et al. [BPB13], which contains four indoor scenes with each scene consisting of a series of images captured with a tripod mounted camera from a static scene with different illuminations. The basic idea is that the estimated reflectance from all the images in each scene should be the same. We measure this by using the mean pixel reconstruction error (MPRE) [ZKE15], which is defined as follows:

$$\text{MPRE}(\{I_i, R_i, S_i\}_{i=1}^N) = \frac{1}{N^2} \sum_{i=1}^N \sum_{j=1}^N E_{\text{si}}(S_i \cdot R_j, I_i), \quad (8)$$

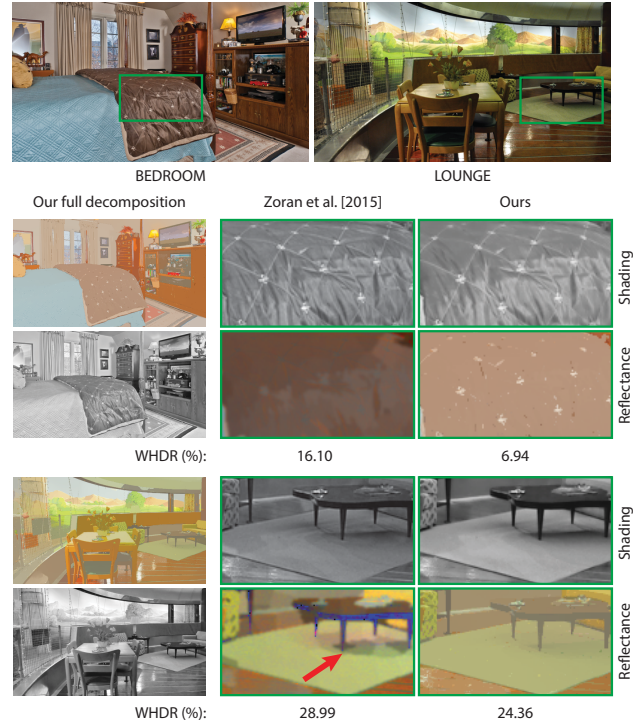


**Figure 10:** Comparison against Zoran et al.’s method [ZIKF15] on two images from the IIW dataset.

where  $E_{\text{si}}$  is the scale invariant MSE, which is defined in Eq. 3. Note that unlike Zhou et al. [ZKE15], here we use the scale invariant MSE as the output of different algorithms could potentially have different scales. We resize each input image so that its larger dimension size is equal to 640.

The MPRE scores for all the approaches on the four scenes are reported in Table 2. As can be seen, our method produces significantly lower MPRE scores, which demonstrates the robustness of our approach to illumination variations. We show two images from the CAFE scene in Fig. 11. Here, we compare all the methods by swapping their estimated reflectance images for the two scenes and multiplying them with the estimated shading images. The result of this process should be close to the original input images. As shown in the insets, our results are closer to the ground truth both visually and numerically. However, other methods struggle to produce comparable results to the ground truth. For example, in the top row, Nestmeyer and Gehler produce results with discoloration. On the other hand, Bi et al., Zhou et al., and Zoran et al. reconstruct images with incorrect shadows under the table.

*Comparison on Surface Retexturing* – With the shading information from intrinsic decomposition results, we can modify the textures of the input images and achieve realistic image editing by multiplying the new texture by the estimated shading. In Figure 12, we change the texture of the sofa and compare the texture editing results with the shading layer estimated with different approaches. From the figure, we can clearly see that Bi et al. and Shi et al. have incorrect lighting on the retextured areas and the retextured images



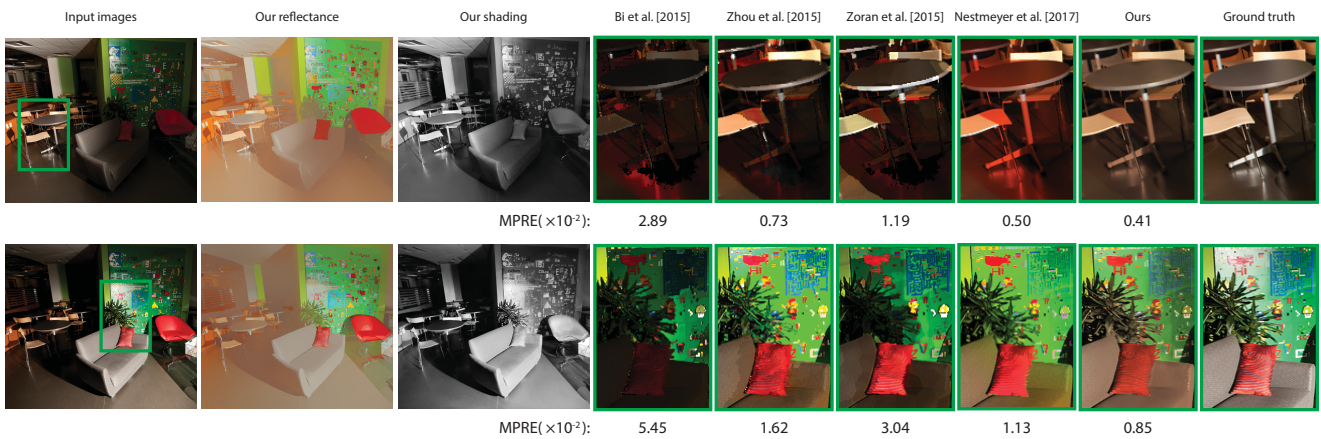


**Figure 11:** On the left, we show two images of the same scene taken under different illumination conditions, and our estimated reflectance and shading images. We show the result of swapping the reflectance images of the two inputs, and multiplying them with the estimated shading of each algorithm in the insets. Our approach produces better results than other methods both visually and numerically.

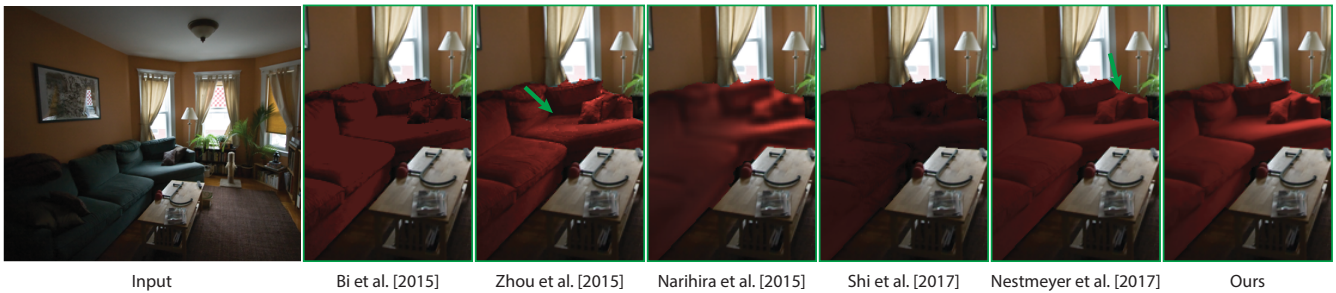


**Figure 12:** Comparisons on surface retexturing results. From the figure we can see that Bi et al. and Shi et al. cannot recover correct shading information at the retextured areas. Narihira et al. produce blurry results. Zhou et al. have obvious discontinuities and artifacts on the sofa surface, and Nestmeyer et al. miss the highlights on the sofa close to the window (as indicated by arrows). In comparison, our method is able to achieve realistic retexturing results without noticeable artifacts.

	Cafe	Kitchen	Sofas	Uris
Bi (2015)	4.47	4.13	3.48	3.28
Narihira (2015)	1.50	1.01	0.87	1.11
Zhou (2015)	1.68	0.87	0.49	0.92
Zoran (2015)	3.49	2.16	1.71	2.09
Shi (2017)	3.80	3.98	4.88	2.96
Nestmeyer (2017)	2.30	0.63	0.42	0.66
Ours	<b>0.68</b>	<b>0.57</b>	<b>0.39</b>	<b>0.46</b>

**Table 2:** Quantitative comparison against other methods in terms of mean pixel reconstruction error on four scenes from Boyadzhiev et al. [BPB13]. We factor out  $10^{-2}$  from all the values for clarity.

look unrealistic. Narihira et al. produces blurry results. Zhou et al. is able to preserve the original lighting conditions, but it also incorrectly preserves the textures in the input image, and therefore there are obvious discontinuities and artifacts on the sofa. Nestmeyer’s results miss the highlights on the sofa close to the window. In com-

parison, our method recovers the lighting information of the input image correctly and achieves realistic retexturing results without noticeable artifacts.

*Runtime Analysis* – During testing, our approach takes 1.4 seconds to process an input image of size  $1280 \times 720$  on an Intel quad-core 3.6 GHz machine with 16 GB memory and a GTX 1080Ti, in which 0.9 seconds is for the bilateral solver. Our timing is comparable to DL-methods such as Shi et al. [SDSS17] and Narihira et al. [NMY15], while is significantly faster than non-DL methods, which take minutes for optimization and post-filtering.

#### 4.2. Comparisons on synthetic images

Here, we compare our approach against other methods on the test images from the Sintel dataset. Table 3 shows the error for both reflectance and shading images using the scale invariant MSE (si-MSE) and local scale invariant MSE (si-LMSE) [GJAF09], a commonly-used metric for quality evaluation on synthetic images. Note that the goal of our approach is producing high-quality de-

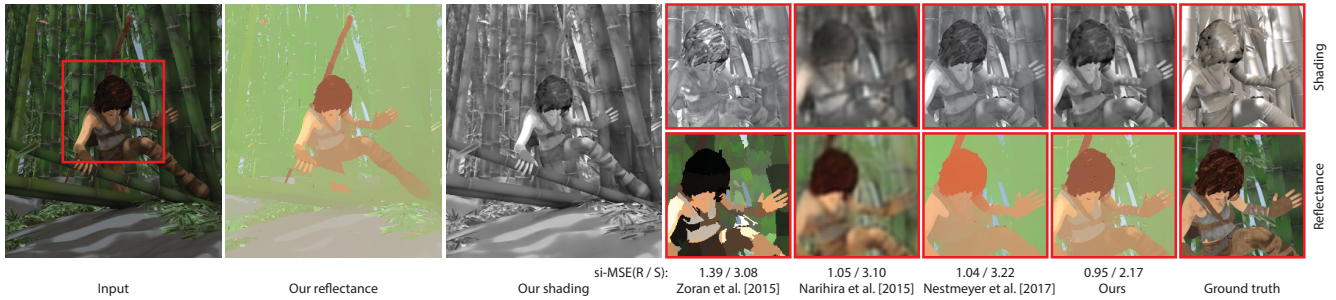


Figure 13: Comparison against the other methods on a test image from the Sintel dataset.

	si-MSE		si-LMSE	
	$R$	$S$	$R$	$S$
Bi (2015)	3.00	3.81	1.48	1.98
Narihira (2015)	<b>2.01</b>	2.24	1.31	1.48
Zhou (2015)	4.02	5.76	2.30	3.63
Zoran (2015)	3.67	2.96	2.17	1.89
Shi (2017)	5.02	4.55	3.52	2.79
Nestmeyer (2017)	2.18	2.16	1.44	1.56
Ours	2.02	<b>1.84</b>	<b>1.30</b>	<b>1.28</b>

Table 3: We compare all the approaches in terms of scale invariant MSE (si-MSE) and local scale invariant MSE (si-LMSE) [GJAF09] on the test scenes from the Sintel dataset. We evaluate the error between the estimated and ground truth reflectance,  $R$ , and shading,  $S$ , images. We factor out  $10^{-2}$  from all values for clarity.

	si-MSE		si-LMSE	
	$R$	$S$	$R$	$S$
Bi (2015)	18.54	17.51	3.11	5.56
Narihira (2015)	7.69	8.69	1.85	2.67
Zhou (2015)	5.51	7.51	1.66	4.19
Zoran (2015)	14.12	12.07	3.69	4.82
Shi (2017)	21.93	20.07	10.03	6.28
Nestmeyer (2017)	<b>5.01</b>	7.06	1.57	3.99
Ours	5.02	<b>6.61</b>	<b>1.41</b>	<b>2.43</b>

Table 4: We report si-MSE and si-LMSE scores of all approaches on the synthetic scenes from the Bonneeel dataset. We factor out  $10^{-2}$  from all values for clarity.

compositions on real images. In contrast to the approaches by Narihira et al. and Shi et al. that only use synthetic images for training, we train our system on both synthetic and real images. Therefore, we did not expect our system to perform better than these methods on synthetic images. Nevertheless, we achieve state of the art accuracies even on this dataset, which demonstrates that our proposed hybrid training does not significantly reduce the accuracy on synthetic images. Compared to other approaches, our method produces significantly better scores. We also show the results of all the approaches on one of the Sintel images in Fig. 13. Zoran et al.’s method produces results with noticeable discontinuities across super-pixel boundaries. Narihira et al. is able to capture the overall structure of reflectance, although generating blurrier results than ours. Finally, Nestmeyer and Gehler’s method is not able to reconstruct the fine details on the cloth.

Moreover, we do another comparison on the synthetic dataset from Bonneeel et al. [BKP17], and report the scores in Table 4. None of the methods in comparison train on this dataset. Different from the testing protocol used by Bonneeel et al., we use the same set of parameters for all scenes instead of picking the best parameters for each scene. Overall our approach produces results with higher accuracy than the other methods.

### 4.3. Limitations

Although our method produces better results than other approaches, in some cases it fails to fully separate the texture where there are large reflectance changes from illumination. The LIVING ROOM scene in Figure 9 is an example of such a case where the texture appears in the estimated shading image by our approach as well as all the other methods. Despite this, our algorithm still produces visually better results than the competing approaches. Moreover, in our current system we assume that the lighting is achromatic, which is not a correct assumption in some cases. In the future, we would like to extend our system to work with colored light sources.

## 5. Conclusions and Future Work

We have presented a hybrid learning approach for intrinsic decomposition by training a network on both synthetic and real images in an end-to-end fashion. Specifically, we train our network on real image pairs of the same scene under different illumination by enforcing the estimated reflectance images to be the same. Moreover, to improve the visual coherency of our estimated reflectance images, we propose to incorporate a bilateral solver as one of the network’s layers during both training and test stages. We demonstrate that our network is able to produce better results than the state-of-the-art methods on a variety of synthetic and real datasets.

In the future, it would be interesting to apply similar ideas to more complex imaging models such as decomposing an image into reflectance, shading, as well as specular layers. Moreover, we

would like to explore the possibility of using the proposed hybrid training for other tasks, such as BRDF and surface normal estimation, where obtaining ground truth on real images is difficult.

## Acknowledgments

This work was supported in part by NSF grant 1617234, ONR grant N000141712687, a Google Research Award, and the UC San Diego Center for Visual Computing.

## References

- [BBS14] BELL S., BALA K., SNAVELY N.: Intrinsic images in the wild. *ACM TOG* 33, 4 (July 2014), 159:1–159:14. 1, 2, 3, 5, 6
- [BHY15] BI S., HAN X., YU Y.: An  $L_1$  image transform for edge-preserving smoothing and scene-level intrinsic decomposition. *ACM TOG* 34, 4 (August 2015), 78:1–78:12. 3, 5, 6
- [BKPB17] BONNEEL N., KOVACS B., PARIS S., BALA K.: Intrinsic decompositions for image editing. *Comput. Graph. Forum* 36, 2 (2017), 593–609. 2, 10
- [BM15] BARRON J. T., MALIK J.: Shape, illumination, and reflectance from shading. *PAMI* 37, 8 (2015), 1670–1687. 3
- [BP16] BARRON J. T., POOLE B.: The fast bilateral solver. *ECCV* (2016). 4
- [BPB13] BOYADZHIEV I., PARIS S., BALA K.: User-assisted image compositing for photographic lighting. *ACM TOG* 32, 4 (2013), 36:1–36:12. 8, 9
- [BPD09] BOUSSEAU A., PARIS S., DURAND F.: User-assisted intrinsic images. *ACM Trans. Graph* 28, 5 (2009), 130:1–130:10. 2
- [BST\*14] BONNEEL N., SUNKAVALLI K., TOMPKIN J., SUN D., PARIS S., PFISTER H.: Interactive intrinsic video editing. *ACM TOG* 33, 6 (2014). 2
- [BT78] BARROW H. G., TENENBAUM J. M.: Recovering intrinsic scene characteristics from images. In *CVS78* (1978), pp. 3–26. 2
- [BWSB12] BUTLER D. J., WULFF J., STANLEY G. B., BLACK M. J.: A naturalistic open source movie for optical flow evaluation. In *ECCV* (2012), Part IV, LNCS 7577, Springer-Verlag, pp. 611–625. 3
- [CFG\*15] CHANG A. X., FUNKHOUSER T., GUIBAS L., HANRAHAN P., HUANG Q., LI Z., SAVARESE S., SAVVA M., SONG S., SU H., XIAO J., YI L., YU F.: *ShapeNet: An Information-Rich 3D Model Repository*. Tech. Rep. arXiv:1512.03012 [cs.GR], 2015. 3
- [CK13] CHEN Q., KOLTUN V.: A simple model for intrinsic image decomposition with depth cues. In *ICCV* (2013), pp. 241–248. 2
- [EPF14] EIGEN D., PUHRSCH C., FERGUS R.: Depth map prediction from a single image using a multi-scale deep network. In *Advances in neural information processing systems* (2014), pp. 2366–2374. 3
- [GJAF09] GROSSE R. B., JOHNSON M. K., ADELSON E. H., FREEMAN W. T.: Ground truth dataset and baseline evaluations for intrinsic image algorithms. In *ICCV* (2009), pp. 2335–2342. 9, 10
- [GMLMG12] GARCES E., MUNOZ A., LOPEZ-MORENO J., GUTIERREZ D.: Intrinsic images by clustering. *Computer Graphics Forum (Proc. EGSR 2012)* 31, 4 (2012). 3
- [GRK\*11] GEHLER P. V., ROTHER C., KIEFEL M., ZHANG L., SCHÖLKOPF B.: Recovering intrinsic images with a global sparsity prior on reflectance. In *NIPS* (2011), pp. 765–773. 4
- [Hor74] HORN B. K. P.: Determining lightness from an image. *Computer Graphics and Image Processing* 3, 1 (Dec. 1974), 277–299. 2
- [HWBS16] HAUAGGE D. C., WEHRWEIN S., BALA K., SNAVELY N.: Photometric ambient occlusion for intrinsic image decomposition. *PAMI* 38, 4 (2016), 639–651. 2
- [IRWM17] INNAMORATI C., RITSCHEL T., WEYRICH T., MITRA N. J.: Decomposing single images for layered photo retouching. In *Computer Graphics Forum* (2017), vol. 36, Wiley Online Library, pp. 15–25. 2
- [KB14] KINGMA D. P., BA J.: Adam: A method for stochastic optimization. *ICLR abs/1412.6980* (2014). 4
- [LBP\*12] LAFFONT P.-Y., BOUSSEAU A., PARIS S., DURAND F., DRETTAKIS G.: Coherent intrinsic images from photo collections. *ACM TOG* 31, 6 (2012), 202:1–202:11. 2, 4
- [LM71] LAND E. H., MCCANN J. J.: Lightness and retinex theory. *Journal of the Optical Society of America* 61, 1 (1971), 1–11. 2
- [MZRT16] MEKA A., ZOLLHÖFER M., RICHARDT C., THEOBALT C.: Live intrinsic video. *ACM TOG* 35, 4 (2016). 2
- [NG17] NESTMEYER T., GEHLER P. V.: Reflectance adaptive filtering improves intrinsic image estimation. In *CVPR* (July 2017), pp. 1771–1780. 1, 2, 3, 5, 6
- [NMY15] NARIHIRA T., MAIRE M., YU S. X.: Direct intrinsics: Learning albedo-shading decomposition by convolutional regression. In *ICCV* (2015), pp. 2992–2992. 1, 2, 3, 6, 9
- [OW04] OMER I., WERMAN M.: Color lines: Image specific color representation. 3
- [SB97] SMITH S. M., BRADY J. M.: Susan—a new approach to low level image processing. *IJCV* 23, 1 (May 1997), 45–78. 4
- [SDSS17] SHI J., DONG Y., SU H., STELLA X. Y.: Learning non-lambertian object intrinsics across shapenet categories. In *CVPR* (2017), pp. 5844–5853. 1, 2, 3, 6, 9
- [SGW\*18] SRINIVASAN P. P., GARG R., WADHWA N., NG R., BARRON J. T.: Aperture supervision for monocular depth estimation. *CVPR* (2018). 5
- [STL08] SHEN L., TAN P., LIN S.: Intrinsic image decomposition with non-local texture cues. In *CVPR* (2008), pp. 1–7. 2
- [TFA05] TAPPEN M. F., FREEMAN W. T., ADELSON E. H.: Recovering intrinsic images from a single image. *PAMI* 27, 9 (Sept. 2005), 1459–1472. 2
- [TM98] TOMASI C., MANDUCHI R.: Bilateral filtering for gray and color images. In *ICCV* (Washington, DC, USA, 1998), ICCV '98, IEEE Computer Society, pp. 839–. 4
- [Wei01] WEISS Y.: Deriving intrinsic images from image sequences. In *ICCV* (2001), pp. II: 68–75. 4
- [ZIKF15] ZORAN D., ISOLA P., KRISHNAN D., FREEMAN W. T.: Learning ordinal relationships for mid-level vision. In *ICCV* (2015), pp. 388–396. 2, 6, 8
- [ZJRP\*15] ZHENG S., JAYASUMANA S., ROMERA-PAREDES B., VIÑEET V., SU Z., DU D., HUANG C., TORR P. H. S.: Conditional random fields as recurrent neural networks. In *ICCV* (2015), pp. 1529–1537. 5
- [ZKE15] ZHOU T., KRÄHENBÜHL P., EFROS A. A.: Learning data-driven reflectance priors for intrinsic image decomposition, 2015. ICCV. 1, 2, 3, 6, 8
- [ZTD\*12] ZHAO Q., TAN P., DAI Q., SHEN L., WU E., LIN S.: A closed-form solution to retinex with nonlocal texture constraints. *IEEE Trans. Pattern Anal. Mach. Intell* 34, 7 (2012), 1437–1444. 2